A New Perspective on the Operating Principle of Flux-Switching Permanent-Magnet Machines

Yujun Shi, *Member, IEEE*, Linni Jian, *Senior Member, IEEE*, Jin Wei, Ziyun Shao, *Member, IEEE*, Wenlong Li, and C. C. Chan, *Fellow, IEEE*

***Abstract*—The flux-switching permanent-magnet (FSPM) machine attracts increasing attention recently due to its high power density, robust mechanical structure, good flux-weakening capability, and essential sinusoidal back-electromotive-force waveforms. In previous studies, the approach for analyzing FSPM machines is either by using the lumped parameter magnetic circuit models or from the "generator-oriented" perspective. In this paper, the operating principle of FSPM machines is reiterated from a new perspective, viz., the "motor-oriented" perspective. Some interesting findings and essential principles can be unveiled, which include how the stable electromagnetic torque can be developed, how the pole-pair number (PPN) of armature windings, the PPN of PMs, and the synchronous speed of the armature field should be defined, and how to determine the connection of coils for the sake of developing stable electromagnetic torques. This new perspective is more consistent with the classical theory on electric machines. There is no need to consider the polarity of coils when determining the connection of windings. Three typical FSPM machines with different combinations of stator and rotor poles, viz., 12/11-pole, 12/13-pole, and 12/26-pole, are investigated to verify the validity of the proposed analysis approach. Experimental verification concerning the latter two sample machines is also conducted.**

***Index Terms*—Electrical motor, field modulation, flux switching, permanent magnet (PM).**

I. Introduction

IN GENERAL, according to the location of permanent magnets (PMs), PM brushless (PMBL) machines can be classified into two types: One is the rotor type (RT), and the other is the stator type (ST) [1]. So far, due to the distinct features in power density and efficiency, RT-PMBL machines have been investigated for several decades, and the relevant technologies have become quite mature. However, RT-PMBL machines, particularly the surface-mounted PM machines, still suffer from the problem of centrifugal force in case of high-speed operation. Therefore, some appropriate measures need to be taken for holding them firmly, for example, sleeve and fixture made of nonmagnetic materials should be adopted. This may lead to a complicated mechanical structure and a relatively large air gap. In contrast, interior RT-PMBL machines are more suitable for high-speed occasions due to their robust structure and inherent flux-weakening capability [2]. Nevertheless, the cooling of RT-PMBL machines is always a headache problem, namely, the overheating of the rotor may result in irreversible demagnetization of the PMs equipped on it.

As far as ST-PMBL machine is concerned, the aforementioned problems can be greatly relieved since it has both the armature windings and PMs installed on the stator. The single-phase ST-PMBL machine was first proposed in 1955 [3]. However, due to the low energy density of PM material at that time, it received little attention. With the advent of high-performance PM material as well as the development of power electronics technology, three novel topologies of ST-PMBL machines were proposed in recent years, including doubly salient PM machines [4], [5], flux reversal machines [6], and multiphase flux-switching PM (FSPM) machines [7]. As illustrated in Fig. 1, the rotor of the FSPM machine only consists of iron laminations, while its stator consists of laminated U-shaped segments

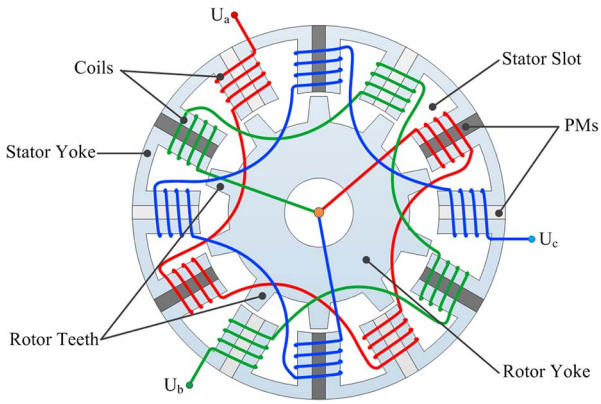

Fig. 1. Topology of FSPM machine with all poles wound.

Manuscript received April 7, 2015; revised June 24, 2015; accepted September 9, 2015. Date of publication October 19, 2015; date of current version February 8, 2016. This work was supported in part by the National Natural Science Foundation of China under Project 51377158, in part by the Natural Science Foundation of Guangdong Province, China, under Project 2014A030306034, and in part by the Science and Technology Innovation Committee of Shenzhen, China, under Project KQCX20140522151322948.

Y. Shi, L. Jian, and J. Wei are with the Department of Electrical and Electronic Engineering, South University of Science and Technology of China, Shenzhen 518055, China (e-mail: shiyj3@mail.sustc.edu.cn; jianln@sustc.edu.cn; weij3@mail.sustc.edu.cn).

Z. Shao is with the School of Mechanical and Electrical Engineering, Guangzhou University, Guangzhou 510006, China (e-mail: zyshao@gzhu.edu.cn).

W. Li and C. C. Chan are with the Department of Electrical and Electronic Engineering, The University of Hong Kong, Hong Kong, China (e-mail: wlli@eee.hku.hk; ccchan@eee.hku.hk).

Color versions of one or more of the figures in this paper are available online at http://ieeexplore.ieee.org.

Digital Object Identifier 10.1109/TIE.2015.2492940

and PMs which are tangentially magnetized and sandwiched in between adjacent U-shaped segments. Each coil is wound around a stator pole. Hence, the mechanical structure of the FSPM machine is simple and robust, and therefore, it is a strong competitor for high-speed applications [8], [9].

With respect to the analysis of FSPM machines, the previous literatures mainly focused on two approaches: One is to establish nonlinear adaptive lumped parameter magnetic circuit models of FSPM machines [10]. It has exhibited high accuracy in predicting the electromagnetic performance of FSPM machines. However, it involves many magnetic circuit models with the rotor in different positions and a series of complicated mathematical calculations. The other is from the so-called "generator-oriented" perspective to interpret how the FSPM machines achieve electromechanical energy conversion [11]. Specifically, by keeping the machine at no load, the flux linkage of each coil can be obtained with the rotor rotating at a constant speed. After that, the voltage induced in each coil can be derived as per Faraday's law of electromagnetic induction. Finally, the connection of coils can be determined in order to ensure the symmetric distribution of the phase back electromotive force (back EMF) waveforms in the time domain. Apparently, this is a typical process for analyzing how electricity is produced in electric generators. However, due to their merits of high power density and efficiency, FSPM machines often work as electric motors in many industrial applications. As for electric motors, what matters the most should be how the electromagnetic torques can be developed and how to improve the performance of the output torques. Unfortunately, the aforementioned generator-oriented perspective can hardly reveal intuitive knowledge on these issues.

In this paper, the operating principle of FSPM machines will be reiterated from a new perspective, viz., the "motor-oriented" perspective. Compared with the existing "generator-oriented" perspective, some interesting findings and essential principles concerning FSPM motors can be unveiled, which include by the interactions of what kind of magnetic field harmonics the stable electromagnetic torque can be developed, how the pole-pair number (PPN) of armature windings and the synchronous speed of the armature field should be defined, and how to determine the connection of coils for the sake of developing stable electromagnetic torques.

II. Operating Principle Analysis From Generator-Oriented Perspective

In this section, the FSPM machines are analyzed from the "generator-oriented" perspective, which is based on the fundamental principle of Faraday's law. For simplicity, an arbitrary coil X illustrated in Fig. 2 is taken for example to explain how electrical power is produced.

As shown in Fig. 2(a), when the rotor locates at position A, the rotor teeth is aligned with the stator teeth, and the magnetic resistance becomes the minimum. Therefore, all the magnetic flux lines go through coil X from the stator to rotor, and the PM flux linkage of coil X reaches its maximum value. This is corresponding to the value of the $\phi_{\rm PM} - \theta_r$ curve with $\theta_r = $ A. Then, when the rotor moves to position B, the rotor teeth is

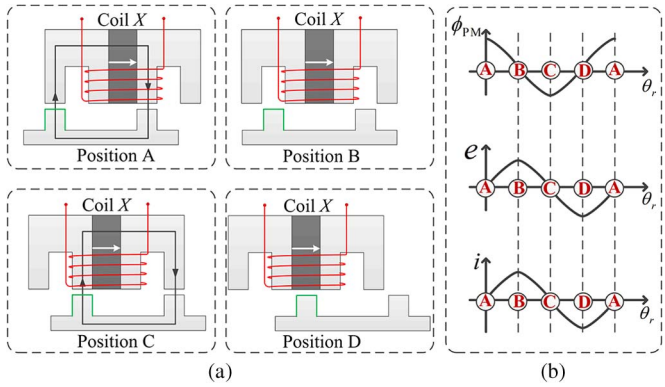

Fig. 2. Operating principle of FSPM machines from generator-oriented perspective. (a) Rotor at four typical positions. (b) Ideal PM flux-linkage, back-EMF, and phase-current waveforms (from top to bottom).

aligned with the stator slots, and the magnetic resistance becomes the maximum. Neglecting the flux leakage, no magnetic flux lines could go through coil X, and this is corresponding to the value of the $\phi_{\rm PM} - \theta_r$ curve with $\theta_r = $ B. Next, when the rotor moves to position C, the rotor teeth is aligned with the stator teeth once again, and the magnetic resistance becomes the minimum. Therefore, all the magnetic flux lines go through coil X from the rotor to stator, and the PM flux linkage of coil X reaches its maximum value. However, it should be noted that the direction of the magnetic flux lines going through coil X has made a change compared with that in the case of position A. Therefore, the PM flux linkage of coil X is the negative maximum, which is corresponding to the value of the $\phi_{\rm PM} - \theta_r$ curve with $\theta_r = $ C. Finally, when the rotor moves to position D, the rotor teeth is aligned with two PMs. Since the permeability of PMs is equal to that of the vacuum, the magnetic resistance becomes the maximum once again, and no magnetic flux lines could go through coil X. This is corresponding to the value of the $\phi_{\rm PM} - \theta_r$ curve with $\theta_r = $ D. So far, a complete period has been depicted. If the rotor continues rotating, exactly the same process will be repeated. It can be observed from the $\phi_{\rm PM} - \theta_r$ curve that the PM flux linkage going through coil X varies with the relative position between the rotor teeth and the stator teeth; moreover, the polarity of PM flux linkage changes once in a cycle. According to Faraday's law of electromagnetic induction, the back-EMF waveform illustrated in Fig. 2(b) can be induced in coil X.

In the classical theory of electric machines, the winding connections of each phase should be determined from the spatial distribution of the coil-EMF vectors, so as to ensure symmetry among the phases. As for FSPM machines, this principle is also expected to be observed. In terms of the $N_{\rm s}/N_{\rm r}$ FSPM machine, the electrical degree α between any two adjacent coil-EMF vectors can be determined in the light of the following formula [12]:

$$\alpha = \frac{360^\circ}{N_s} N_r \tag{1}$$

where N_s denotes the number of stator slots, which is also equal to the number of stator poles; N_r indicates the number of rotor poles, which is also equal to the number of rotor teeth.

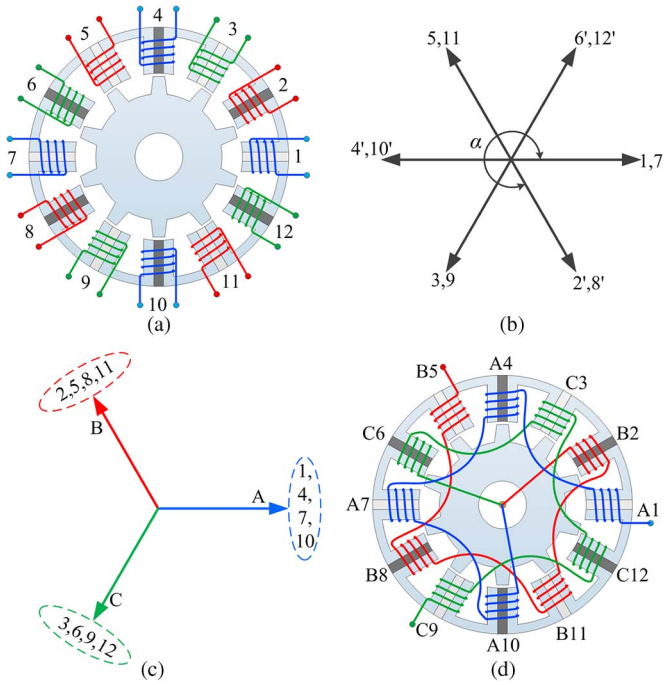

Fig. 3. Three-phase 12/10 FSPM machine. (a) Numbered coils on stator. (b) Coil-EMF vectors. (c) Phase coil vectors. (d) Phase winding connection.

It can be observed from (1) that the number of rotor poles N_r in the FSPM machine is equivalent to the PPN of PMs or armature windings in the conventional RT-PMBL machines, such as PM synchronous machines (PMSM) and PM brushless direct current (PMBLDC) machines. Nevertheless, taking the alternate magnetization of PMs on the stator into consideration, any adjacent two coils are with opposite polarity, and this should be clearly indicated when plotting the coil-EMF vectors of FSPM machines. Otherwise, a serious mistake may occur when determining the connection of coils. The electrical frequency f of the electricity generated in the coils is given by

$$f = \frac{N_r \omega_r}{60} \tag{2}$$

where ω_r is the rotational speed of the rotor and its unit is revolutions per minute (r/min).

As shown in Fig. 3, a three-phase 12/10 FSPM machine with all poles wound is chosen to explain how to connect the coils. Fig. 3(a) illustrates the stator and the numbered coils on it. Fig. 3(b) depicts the coil-EMF vectors. The electrical degree between any two adjacent vectors equals 300°, which can be calculated from (1). In addition, special attention should be paid to the fact that the coils No. 1, 3, 5, 7, 9, and 11 are with opposite polarity with the coils No. 2, 4, 6, 8, 10, and 12, and therefore, the vectors No. 2, 4, 6, 8, 10, and 12 are indicated with apostrophes. Finally, the phase coil vectors and the winding connections can be determined as shown in Fig. 3(c) and (d).

III. Operating Principle Analysis From Motor-Oriented Perspective

With no doubt, for any PMBL machine no matter what type it is, it should operate through the interaction of the magnetic fields excited by the PMs and the armature currents, so as to produce electromagnetic torque (for rotary machines) or force (for linear machines). For achieving a stable output torque/force, two conditions should be strictly satisfied: 1) The PPN of the magnetic field excited by the PMs should be equal to that excited by armature currents, and 2) the rotational speeds of the magnetic fields with the same PPN should be equal to each other. For a conventional RT-PMBL machine, such as a PMSM or PMBLDC machine, torque generation depends on the interaction of the magnetic fields in the air gap excited by the armature windings on the stator and the PMs on the rotor. The PPN of armature windings is designed to be the same with the PPN of PMs. What is more, the speed of the rotational magnetic field yielded by armature currents is also equal to that of the rotor PMs, and this is usually corresponding to a vitally important concept named as "synchronous speed." It is worth noting that the RT-PMBL machine generally relies on the coupling of the fundamental components of magnetic fields to produce stable electromagnetic torques. For example, if there are 6 PM poles equipped on the rotor, which means the PPN of PMs equals 3, the armature windings on the stator should be designed to be with PPN = 3. Moreover, the electromagnetic torque is produced through the interaction of the fundamental component (PPN = 3) of the magnetic fields excited by the armature currents and the PMs, and the field harmonics are either neglected or deemed as the contributors to torque ripples or cogging torques.

Nevertheless, for FSPM machines, it is no longer explicit to tell how electromagnetic torque is produced in them. Several key concepts concerning FSPM machines should be reconsidered and rebuilt, for example, the PPN of armature windings, the PPN of PMs, and the synchronous speed of the armature field. Fortunately, enlightened by the operating principle of magnetic gears [13]–[15], the mechanism for generating electromagnetic torque in FSPM machines can be revealed from the motor-oriented perspective. As shown in Fig. 1, the topology of the FSPM machine has prominent salient rotor poles, which gives rise to the noneven magnetic field paths. Similar to the function of the ferromagnetic segments in magnetic gears, these salient poles can excite abundant field harmonics in the air gap of FSPM machines. With the interaction of some specific harmonic components, FSPM machines are able to output stable electromagnetic torque. This operating principle can be expounded by the so-called magnetic gearing effect [16]–[18].

A. How to Define PPNs of PMs and Armature Windings in FSPM Machines?

With regard to a three-phase N_s/N_r FSPM machine with all poles wound, the number of PM poles equipped on the stator is equal to N_s. Without any doubt, it can be obtained that

$$P_s = \frac{N_s}{2} \tag{3}$$

where P_s denotes the PPN of PMs in FSPM machines.

From the generator-oriented perspective introduced in Section II, the number of rotor poles N_r in the FSPM machine

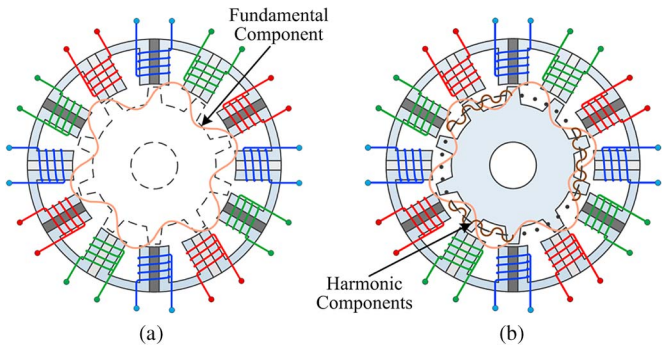

Fig. 4. Magnetic field excited by PMs. (a) Fundamental component without considering the impact of rotor. (b) Field modulation caused by rotor poles.

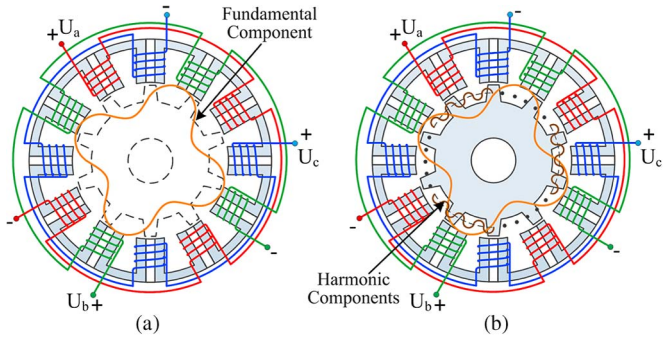

Fig. 5. Magnetic field excited by armature currents. (a) Fundamental component without considering the impact of rotor. (b) Field modulation caused by rotor poles.

is equivalent to the PPN of armature windings in the conventional RT-PMBL machines. However, it is not completely reasonable to consider that the PPN of armature windings in the FSPM machine is equal to N_r since the PPN of PMs should be equal to the PPN of armature windings in conventional machines. That is why we have to pay special attention to the polarity of coils when plotting the coil-EMF vectors. It seems that we have been stuck in a dilemma. Fortunately, enlightened by the magnetic gearing effect, if we define

$$P_w = N_r - P_s \tag{4}$$

where P_w denotes the PPN of armature windings in FSPM machines, we are able to find the way out to figure out how come the electromagnetic torque is generated by the interaction of field harmonics.

B. Field Modulation and Effective Coupling of Field Harmonics in FSPM Machines

The magnetic field produced by the PMs is analyzed. First, as illustrated in Fig. 4(a), the coils are open-circuited, and the rotor is removed. The PPN of the fundamental component of the magnetic field solely excited by the PMs should be equal to P_s, which is defined by (3). Second, as illustrated in Fig. 4(b), the rotor is taken into consideration, but the coils are still open-circuited. Due to the salient rotor poles, the magnetic field excited by the PMs will be modulated. This means that, aside from the fundamental component, there will be a lot of harmonic components existing in the air gap. The PPN of the specific field harmonic denoted by $H_s(i,j)$ can be determined by

$$P^s_{(i,j)} = |iP_s + jN_r| \tag{5}$$

where $i = 1, 3, 5, \ldots, \infty$ and $j = 0, \pm1, \pm2, \pm3, \ldots, \pm\infty$; N_r is the number of rotor poles. Furthermore, its rotational speed can be given by

$$\omega^s_{(i,j)} = \frac{jN_r}{iP_s + jN_r}\omega_r \tag{6}$$

where ω_r is the rotational speed of the rotor. It can be observed that, although the PMs are installed on the stator which is kept at standstill, the field harmonics (when $j \neq 0$) excited by them are still rotating in the air gap due to the rotation of the rotor.

Next, the magnetic field produced by the armature currents is analyzed. First, as illustrated in Fig. 5(a), the coils are injected with symmetric phase currents (sinusoidal ac currents), and both the PMs and the rotor are removed. It is easy to understand that the PPN of the fundamental component of the magnetic field solely excited by the armature windings should be equal to P_w, which is defined by (4). In addition, its rotational speed can be determined by

$$\omega_w = \frac{60f}{P_w} \tag{7}$$

where f denotes the frequency of the injected ac currents and the unit of ω_w is revolutions per minute (r/min). This speed ω_w is also termed as the "synchronous speed of the armature field" in the classical electric machine theory. Second, as illustrated in Fig. 5(b), the rotor is taken into consideration, but the PMs are still removed. Similarly, due to the salient rotor poles, the magnetic field excited by the armature windings will be modulated. This means that, aside from the fundamental component, there will be a lot of harmonic components existing in the air gap. The PPN of the specific field harmonic component denoted by $H_w(m,k)$ can be determined by

$$P^w_{(m,k)} = |mP_w + kN_r| \tag{8}$$

where $m = 1, 3, 5, \ldots, \infty$ and $k = 0, \pm1, \pm2, \pm3, \ldots, \pm\infty$. Furthermore, its rotational speed can be given by

$$\omega^w_{(m,k)} = \frac{mP_w}{mP_w + kN_r}\omega_w + \frac{kN_r}{mP_w + kN_r}\omega_r. \tag{9}$$

Then, the coupling of the magnetic fields excited by the PMs and the armature windings can be discussed. As mentioned earlier, only the field components which are with exactly the same PPN and the same rotational speed can interact with each other to generate stable electromagnetic torque. From (3)–(9), it is easy to know that, as long as the following condition is satisfied:

$$\omega_r = \frac{P_w}{N_r}\omega_w \tag{10}$$

TABLE I
EFFECTIVE COUPLING OF FIELD HARMONICS IN FSPM MACHINES

Effective Harmonic Pairs $[H_s(i,j), H_w(m,k)]$	Pole-pair Number (PPN) $P^s_{(i,j)} = P^w_{(m,k)}$	Rotational Speed $\omega^s_{(i,j)} = \omega^w_{(m,k)}$
$[H_s(1,-1), H_w(1,0)]$	$(P_s - N_r) = P_w$	$\left[-N_r\omega_r/(P_s - N_r)\right] = \omega_w$
$[H_s(1,0), H_w(1,-1)]$	$P_s = \lvert P_w - N_r\rvert$	$0 = \left[(P_w\omega_w - N_r\omega_r)/(P_w - N_r)\right]$
$[H_s(1,-3), H_w(1,2)]$	$\lvert P_s - 3N_r\rvert = \lvert P_w + 2N_r\rvert$	$\left[-3N_r\omega_r/(P_s - 3N_r)\right] = \left[(P_w\omega_w + 2N_r\omega_r)/(P_w + 2N_r)\right]$
$[H_s(3,-3), H_w(3,0)]$	$3(P_s - N_r) = 3P_w$	$\left[-N_r\omega_r/(P_s - N_r)\right] = \omega_w$
$[H_s(3,0), H_w(3,-3)]$	$3P_s = 3\lvert P_w - N_r\rvert$	$0 = \left[(P_w\omega_w - N_r\omega_r)/(P_w - N_r)\right]$
$[H_s(3,-2), H_w(3,-1)]$	$\lvert 3P_s - 2N_r\rvert = \lvert 3P_w - N_r\rvert$	$\left[-2N_r\omega_r/(3P_s - 2N_r)\right] = \left[(3P_w\omega_w - N_r\omega_r)/(3P_w - N_r)\right]$
⋮	⋮	⋮
$[H_s(i,-i), H_w(m,0)]$, $i=m$	$i(P_s - N_r) = mP_w$	$\left[-N_r\omega_r/(P_s - N_r)\right] = \omega_w$
$[H_s(i,0), H_w(m,-m)]$, $i=m$	$iP_s = m\lvert P_w - N_r\rvert$	$0 = \left[(P_w\omega_w - N_r\omega_r)/(P_w - N_r)\right]$
$[H_s(i,j), H_w(m,k)]$, $i=m$, $i=-(j+k)$	$\lvert iP_s + jN_r\rvert = \lvert mP_w + kN_r\rvert$	$\left[jN_r\omega_r/(iP_s + jN_r)\right] = \left[(mP_w\omega_w + kN_r\omega_r)/(mP_w + kN_r)\right]$
⋮	⋮	⋮

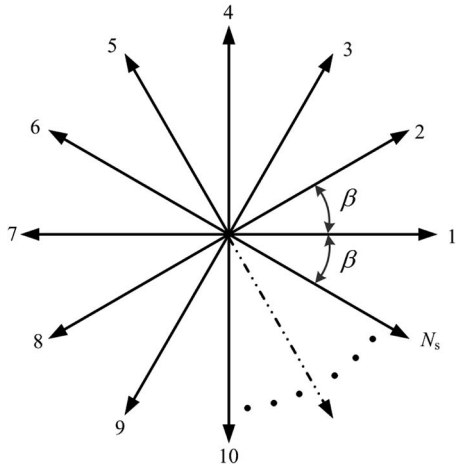

Fig. 6. Coil-EMF vectors of FSPM machine from motor-oriented perspective.

some effective harmonic pairs $[H_s(i,j), H_w(m,k)]$ which are capable of generating stable electromagnetic torques can be identified as listed in Table I.

C. New Winding Connection Approach for FSPM Machines

From the abovementioned motor-oriented perspective, a new winding connection approach for FSPM machines which is in accordance with the classical theory of electric machines can be built up. First, the electrical degree β between any two adjacent coil-EMF vectors can be determined via the following formula:

$$\beta = \frac{360^\circ}{N_s} P_w \tag{11}$$

where P_w is the PPN of armature windings defined in (4) and N_s is the number of coils on the stator.

Second, the coil-EMF vectors can be depicted as illustrated in Fig. 6. Finally, the phase coil vectors and the winding connections can be determined according to the number of winding phases and the symmetry among these phases. More details will be further explained in Section IV.

The key difference between the winding connection approaches concluded from the motor-oriented perspective and the generator-oriented perspective lies in the knowledge on the PPN of armature windings. Comparing (1) and (11), it can be understood that, in the previous literatures, the PPN of armature windings is deemed as the number of rotor teeth N_r equivalently, while, in our proposed approach, the PPN of armature windings is defined by (4). In this way, there is no need to consider the polarity of coils anymore. Apparently, the winding connection approach presented herein is more consistent with the classical theory of electric machines.

D. Summary

In summary, from the proposed motor-oriented perspective, several key issues on FSPM machines can be concluded as follows.

1) FSPM machines are essentially flux-modulated machines. They rely on the magnetic field harmonics to achieve electromechanical energy conversion. The effective harmonic pairs which can generate stable electromagnetic torques are listed in Table I.
2) The PPN of PMs P_s is defined by (3), which is equal to half of the number of stator poles N_s.
3) The PPN of armature windings P_w is defined by (4), which is equal to the difference between the number of rotor poles N_s and the PPN of PMs P_s.
4) When driven by sinusoidal ac phase currents whose frequency is denoted by f, the rotational speed of the rotor of the FSPM machine can be determined by (10).

IV. CASE STUDIES

Several sample machines are quantitatively investigated from the proposed motor-oriented perspective by using the finite

TABLE II
IDENTICAL PARAMETERS OF SAMPLE MACHINES

Number of Phases	3
Magnetic Remanence	1.2 T
Relative PM Permeability	1.05
Outer Radius of Stator	45 mm
Inner Radius of Stator	27.5 mm
Length of Air-gap	0.6 mm
Effective Axial Length	25 mm

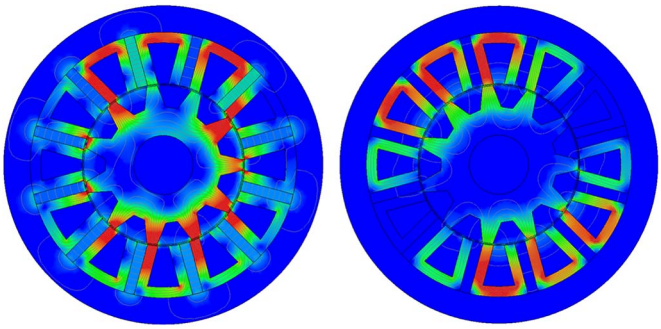

Fig. 7. Field flux line distributions (12/11 FSPM machine). (a) Excited by PMs. (b) Excited by armature currents.

element method (FEM). The topology of these sample machines is similar to that illustrated in Fig. 1, but they are with different combinations of stator and rotor poles. In addition, their identical parameters are listed in Table II.

A. 12/11 FSPM Machine

The field flux line distributions are illustrated in Fig. 7, in which Fig. 7(a) shows the flux distribution solely excited by the PMs while Fig. 7(b) shows that solely excited by the armature currents. Figs. 8 and 9 give the radial flux density waveforms in the air gap and their harmonic spectra built up by the PMs and armature currents, respectively. It can be observed that there are many field harmonics due to the modulation effect arising from the rotor poles. Since the numbers of stator poles and rotor poles are equal to 12 and 11, respectively, the PPN of PMs P_s should be 6, and that of armature windings P_w should be 5, according to (3) and (4). The corresponding fundamental components are indicated in Figs. 8(b) and 9(b). Moreover, the rotational speeds of the field harmonics can be determined by setting the rotor rotating at a constant speed ω_r. Therefore, the effective harmonic pairs which are with the same PPN and the same rotational speed can be identified as illustrated in Fig. 10. The result matches Table I very well. It is worth noting that, for the harmonic pairs with PPN $= 6$, 18, 30, although they keep still all the time, they also can contribute to the stable output torque.

Since the PPN of armature windings P_w is 5, according to (11), the electrical degree β between any two adjacent coil-EMF vectors becomes 150°; thus, the coil-EMF vectors can be plotted as shown in Fig. 11(b). For comparison, the vectors

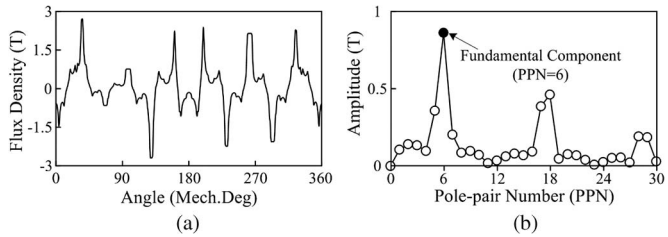

Fig. 8. Flux distribution in air gap excited by PMs (12/11 FSPM machine). (a) Radial flux density waveform. (b) Harmonic spectrum.

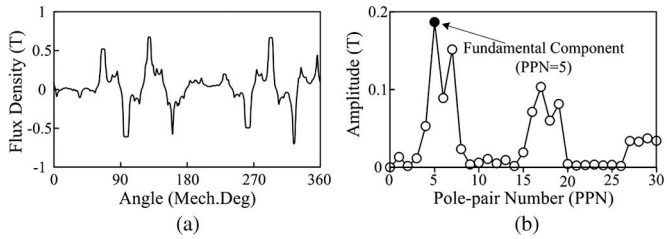

Fig. 9. Flux distribution in air gap excited by armature currents (12/11 FSPM machine). (a) Radial flux density waveform. (b) Harmonic spectrum.

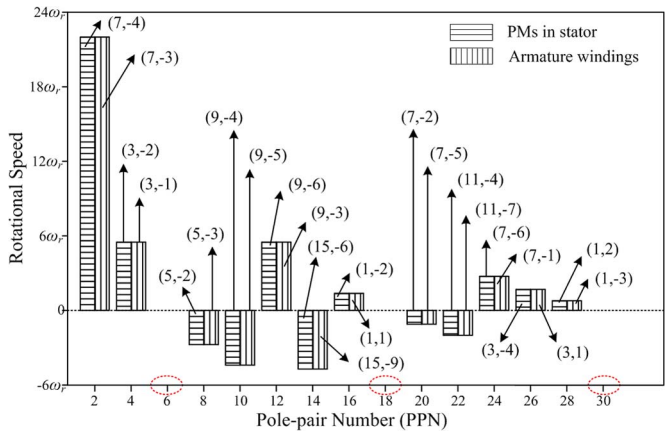

Fig. 10. Effective harmonic pairs (12/11 FSPM machine).

determined from the generator-oriented perspective are given in Fig. 11(a). The electrical degree α between any two adjacent coil-EMF vectors equals 330° according to (1). Regardless if they are determined from the motor-oriented or the generator-oriented perspective, the phase coil vectors and the winding connection are illustrated in Fig. 11(c) and (d). Nevertheless, the polarities of the coils have to be taken into consideration from the generator-oriented perspective, while there is no need to do so from the motor-oriented perspective.

The back-EMF waveforms induced in the coils and phases when the rotor rotates at 10000/11 r/min can be obtained as illustrated in Fig. 12. The number of turns of coils is set to be equal to 1. It can be found that the electric period is 6 ms; hence, the electric frequency is equal to 500/3 Hz, which is in accordance with the result obtained from (2). Then, the synchronous speed of the armature field ω_w is 2000 r/min according to (7). This means that (10) can be satisfied.

The performance of electromagnetic torque is assessed by injecting ac currents into the armature windings. The number of turns of coils is set as 100. The magnitude and the frequency

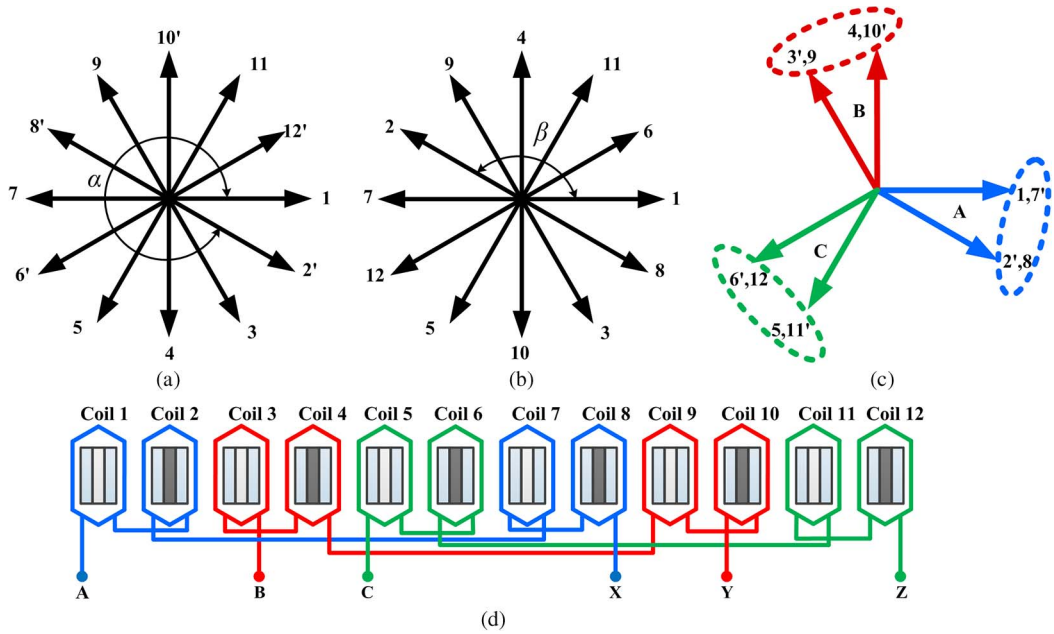

Fig. 11. Winding connection approach (12/11 FSPM machine). (a) Coil-EMF vectors from generator-oriented perspective. (b) Coil-EMF vectors from motor-oriented perspective. (c) Three phase coil vectors. (d) Three phase winding connection.

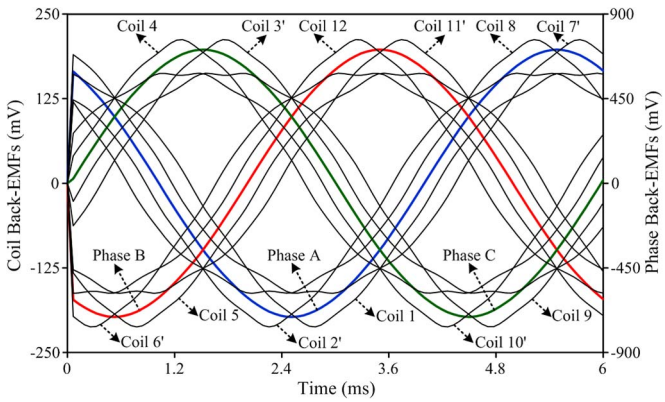

Fig. 12. Back-EMF waveforms of coils and phases (12/11 FSPM machine).

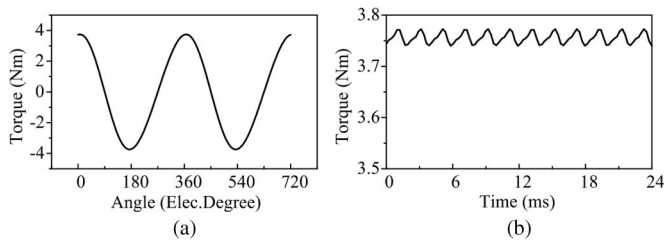

Fig. 13. Performance of electromagnetic torque (12/11 FSPM machine). (a) Torque–angle curve when rotor is kept at standstill. (b) Maximum torque–time waveform with rotor rotating at synchronous speed.

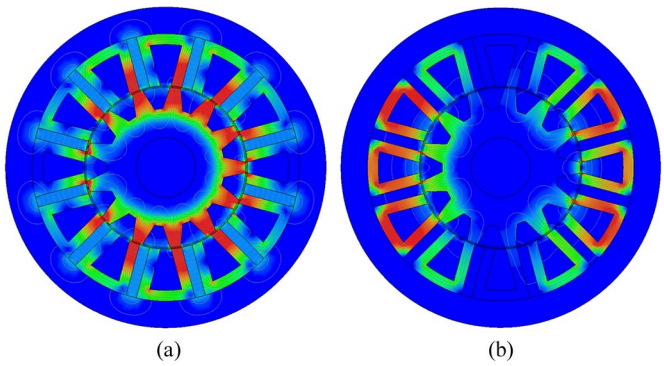

Fig. 14. Field flux line distributions (12/13 FSPM machine). (a) Excited by PMs. (b) Excited by armature currents.

of phase current are set as 3 A and 82.5 Hz, respectively. Therefore, the synchronous speed of the armature field ω_w is equal to 990 r/min according to (7). When the rotor is kept at standstill, the resulted torque–angle curve is shown in Fig. 13(a). It can be observed that the peak value is 3.75 Nm. In addition, the synchronous speed of the rotor ω_r is equal to 450 r/min according to (10). When keeping the rotor rotating at this synchronous speed, the maximum torque–time waveform can be obtained as shown in Fig. 13(b). With ignoring the torque ripple, this can be deemed as the stable electromagnetic torque produced by the effective coupling of field harmonic pairs identified in Fig. 10.

B. 12/13 FSPM Machine

Figs. 14–16 show the field flux line distributions and the flux distributions in the air gap of the 12/13 FSPM machine excited by the PMs and the armature currents. Since the numbers of stator poles and rotor poles are equal to 12 and 13, respectively, the PPN of PMs P_s should be 6, and that of armature windings P_w should be 7, according to (3) and (4). The corresponding fundamental components are indicated in harmonic spectra illustrated in Figs. 15(b) and 16(b). It is worth noting that, in Fig. 16(b), the magnitude of the field component with PPN $= 5$ is even larger than the magnitude of the fundamental component with PPN $= 7$. This phenomenon will be further

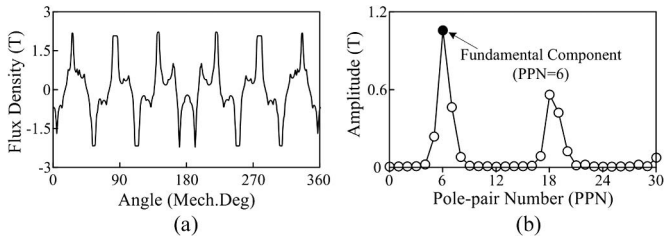

Fig. 15. Flux distribution in air gap excited by PMs (12/13 FSPM machine). (a) Radial flux density waveform. (b) Harmonic spectrum.

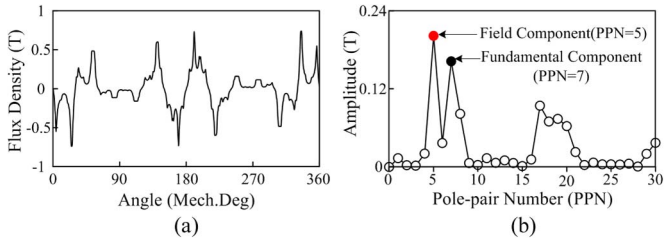

Fig. 16. Flux distribution in air gap excited by armature currents (12/13 FSPM machine). (a) Radial flux density waveform. (b) Harmonic spectrum.

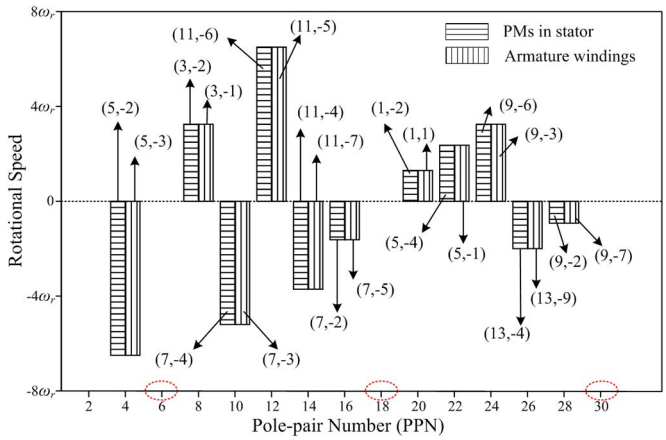

Fig. 17. Effective harmonic pairs (12/13 FSPM machine).

investigated after figuring out how the coils are connected. The rotational speeds of the field harmonics can be determined by setting the rotor rotating at a constant speed ω_r. Therefore, the effective harmonic pairs which are with the same PPN and the same rotational speed can be identified as illustrated in Fig. 17. The result also matches Table I very well.

According to (11), the electrical degree β between any two adjacent coil-EMF vectors becomes 210°; thus, the coil-EMF vectors can be plotted as shown in Fig. 18(b). Similarly, the vectors determined from the generator-oriented perspective are given in Fig. 18(a), in which the electrical degree α between any two adjacent coil-EMF vectors equals 390° or 30° according to (1). The phase coil vectors and the winding connection are illustrated in Fig. 18(c) and (d). Again, it demonstrates that, from the proposed motor-oriented perspective, the winding connections can be correctly determined without considering the polarity of the coils.

Let us go back to Fig. 16(b) to figure out why the magnitude of the field component with PPN $= 5$ is even larger than that of the fundamental component with PPN $= 7$. Assuming that the PPN of armature windings is given as 5, the coil-EMF vectors and the phase coil vectors can be determined as illustrated in Fig. 19. The electrical degree β' between any two adjacent coil-EMF vectors becomes 150°. Comparing Figs. 19(b) and 18(c), it is easy to find that, no matter whether the PPN of armature windings is equal to 5 or 7, the winding connection can be determined as depicted in Fig. 18(d). In other words, once the coils are connected in the way as illustrated in Fig. 18(d), the resulted PPN of armature windings could be 7 or 5; both are reasonable. Nevertheless, it does not hamper the analysis on FSPM machines from the proposed motor-oriented perspective at all, as long as the PPN of armature windings is determined according to (4).

The back-EMF waveforms induced in the coils and phases when the rotor rotates at 10 000/13 r/min can be obtained as illustrated in Fig. 20. The number of turns of coils is also set to be equal to 1. It can be found that the electric period is 6 ms; hence, the electric frequency is equal to 500/3 Hz, which is in accordance with the result obtained from (2). Then, the synchronous speed of the armature field ω_w is 10 000/7 r/min according to (7). This means that (10) can be satisfied.

The performance of electromagnetic torque is depicted in Fig. 21. The number of turns of coils is set as 100. The magnitude and the frequency of injected phase current are set as 3 A and 97.5 Hz, respectively. Hence, the synchronous speeds of armature field ω_w and rotor ω_r are equal to 835.7 and 450 r/min according to (7) and (10), respectively. The resulted torque–angle curve is shown in Fig. 21(a), and the peak value is 4.07 Nm. The maximum torque–time waveform is obtained as shown in Fig. 21(b), and this can be deemed as the stable electromagnetic torque produced by the effective coupling of field harmonic pairs identified in Fig. 17.

C. 12/26 FSPM Machine

In this case, Figs. 22–24 show the field flux line distributions and the flux distributions in the air gap excited by the PMs and the armature currents. Since the numbers of stator poles and rotor poles are equal to 12 and 26, respectively, the PPN of PMs P_s should be 6, and that of armature windings P_w should be 20, according to (3) and (4). The corresponding fundamental components are indicated in harmonic spectra illustrated in Figs. 23(b) and 24(b). The effective harmonic pairs which are with the same PPN and the same rotational speed can be identified as illustrated in Fig. 25. The result also matches Table I very well.

Since the PPN of armature windings P_w is 20, according to (11), the electrical degree β between any two adjacent coil-EMF vectors becomes 600° or 240°; thus, the coil-EMF vectors can be plotted as shown in Fig. 26(b). For comparison, the vectors determined from the generator-oriented perspective are given in Fig. 26(a), in which the electrical degree α between any two adjacent coil-EMF vectors equals 780° or 60° according to (1). The phase coil vectors and the winding connection are illustrated in Fig. 26(c) and (d). It also demonstrates that,

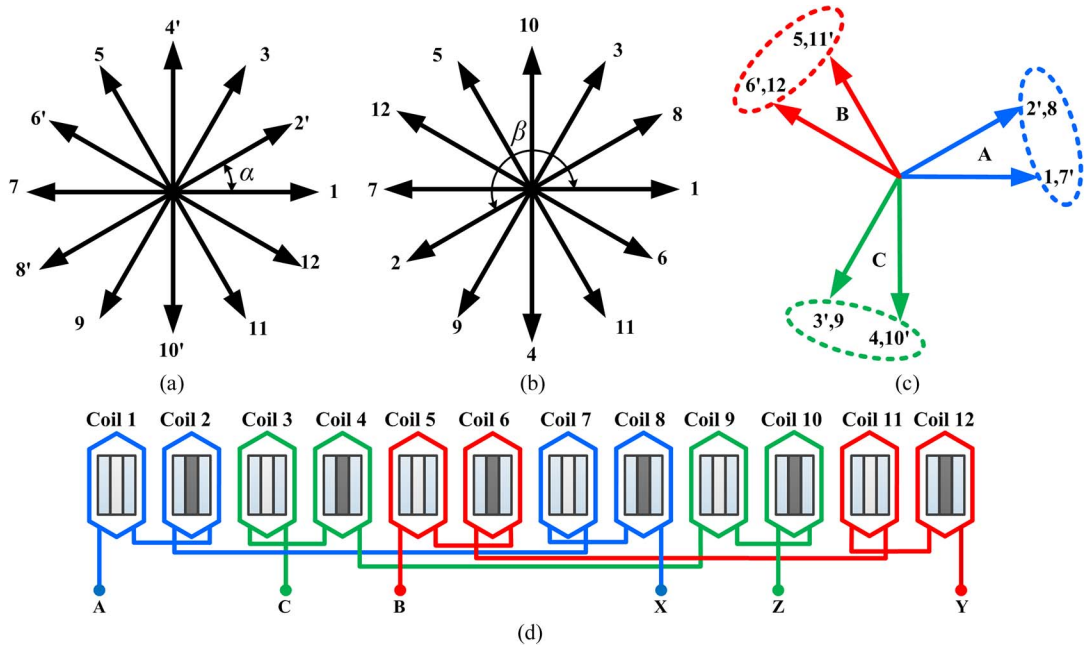

Fig. 18. Winding connection approach (12/13 FSPM machine). (a) Coil-EMF vectors from generator-oriented perspective. (b) Coil-EMF vectors from motor-oriented perspective. (c) Three phase coil vectors. (d) Three phase winding connection.

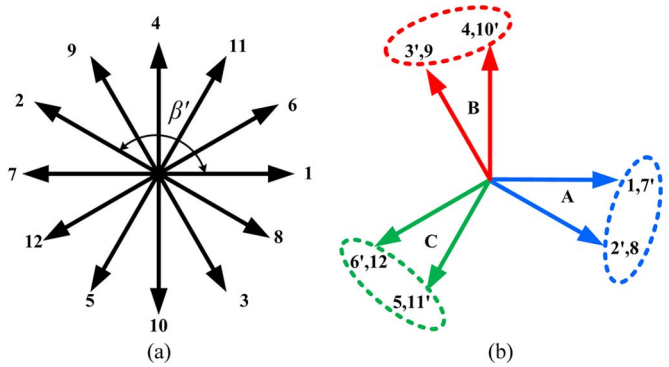

Fig. 19. Winding connection when assuming the winding's PPN equal to 5. (a) Coil-EMF vectors. (b) Three phase coil vectors.

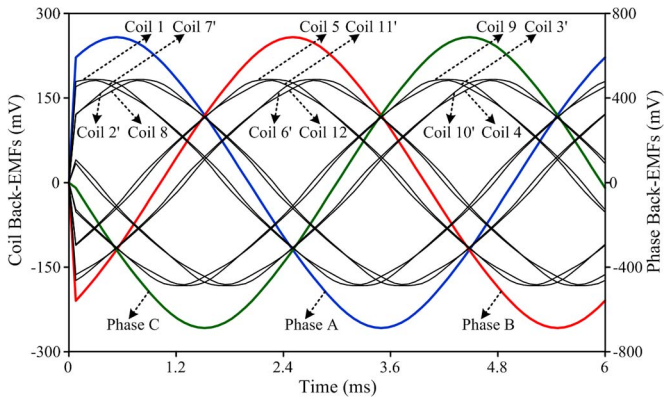

Fig. 20. Back-EMF waveforms of coils and phases (12/13 FSPM machine).

from the proposed motor-oriented perspective, the winding connections can be correctly determined without considering the polarity of the coils.

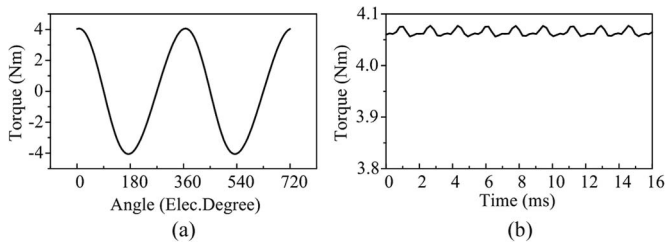

Fig. 21. Performance of electromagnetic torque (12/13 FSPM machine). (a) Torque–angle curve when rotor is kept at standstill. (b) Maximum torque–time waveform with rotor rotating at synchronous speed.

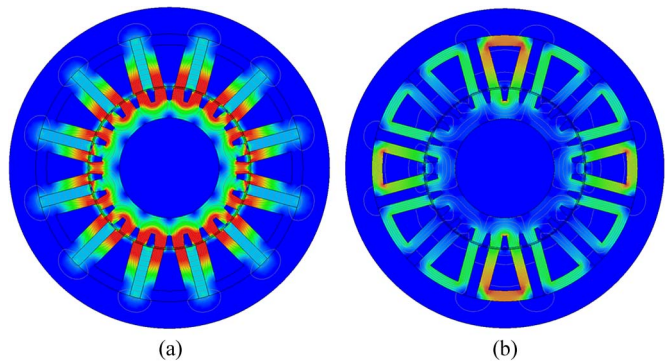

Fig. 22. Field flux line distributions (12/26 FSPM machine). (a) Excited by PMs. (b) Excited by armature currents.

The back-EMF waveforms induced in the coils and phases when the rotor rotates at 450 r/min can be obtained as illustrated in Fig. 27. The number of turns of coils is set to be equal to 1. It can be found that the electric period is 5.13 ms; hence, the electric frequency is equal to 195 Hz, which is in accordance with the result obtained from (2). Then, the synchronous speed

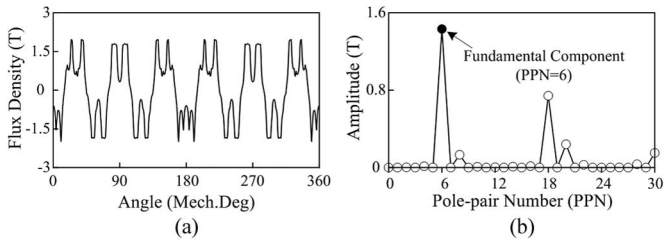

Fig. 23. Flux distribution in air gap excited by PMs (12/26 FSPM machine). (a) Radial flux density waveform. (b) Harmonic spectrum.

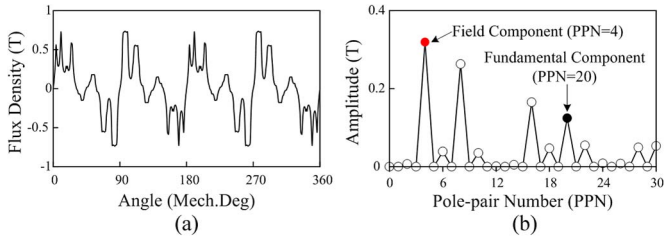

Fig. 24. Flux distribution in air gap excited by armature currents (12/26 FSPM machine). (a) Radial flux density waveform. (b) Harmonic spectrum.

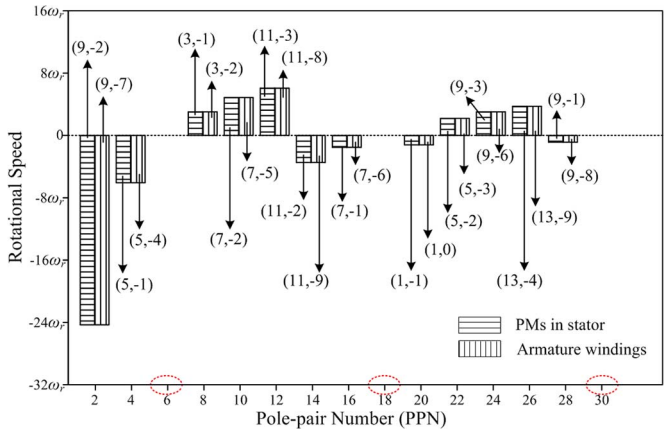

Fig. 25. Effective harmonic pairs (12/26 FSPM machine).

of the armature field ω_w is 585 r/min according to (7). This means that (10) can be satisfied.

The performance of electromagnetic torque is depicted in Fig. 28. The number of turns of coils is set as 100. The magnitude and the frequency of injected phase current are set as 3 A and 195 Hz, respectively. Hence, the synchronous speeds of armature field ω_w and rotor ω_r are equal to 585 and 450 r/min according to (7) and (10), respectively. The resulted torque–angle curve is shown in Fig. 28(a), and the peak value is 248.69 mNm. The maximum torque–time waveform is obtained as shown in Fig. 28(b), and this can be deemed as the stable electromagnetic torque produced by the effective coupling of field harmonic pairs identified in Fig. 25.

D. Comparison

It can be known from the previous literatures that, when the ratio of N_s and N_r is near to 1, the FSPM machine can offer prominent performance [19]. This has been successfully demonstrated by the aforementioned case studies. Comparing Figs. 12, 20, and 27, it can be known that the 12/11 and 12/13 FSPM machines are able to offer much higher back EMFs than the 12/26 FSPM machine. Moreover, Figs. 13, 21, and 28 indicate that the 12/11 and 12/13 FSPM machines are capable of outputting much bigger electromagnetic torques than the 12/26 FSPM machine. With the help of Table III, we can conveniently investigate all kinds of possible combinations of numbers of stator poles and rotor poles. Herein, the number of stator poles N_s is kept as 12, while the number of rotor poles N_r ranges from 1 to 26. The PPN of PMs (P_s), the PPN of armature windings (P_w), and the electrical degree between any two adjacent coil-EMF vectors (β) can be determined by (3), (4), and (11), respectively. For cases $N_r = 1$–6, the resulted PPN of armature windings is negative or zero, which means that these combinations are infeasible. What is more, for cases $N_r = 9$, 12, 15, 18, 21, and 24, the resulted electrical degree between any two adjacent coil-EMF vectors equals 0°, 90°, 180°, or 270°, which means that the stator coils cannot form three-phase symmetric windings. Therefore, the remaining 14 possible combinations are chosen for further investigation.

Fig. 29 shows the comparison of performance of these 14 cases, in which Fig. 29(a) gives the peak values of stable electromagnetic torques while Fig. 29(b) gives the magnitudes of phase back EMFs when rotors rotate at 450 r/min. All these results are calculated by using the FEM. It can be observed that the two curves in Fig. 29 have similar patterns, and for cases in which N_r is close to N_s, such as 12/10, 12/11, 12/13, and 12/14, they definitely outperform the other cases. In order to figure out the essential reasons behind this phenomenon, the magnetic field distributions and their harmonic spectra in the air gaps of these sample machines are investigated, and the results have been plotted in Fig. 30. The green curve indicates the magnitudes of the harmonic components with PPN $= P_w$ excited by the PMs in these sample machines. The red curve indicates the magnitudes of the fundamental components with PPN $= P_w$ excited by the armature currents in these sample machines. From the proposed motor-oriented perspective, the field harmonic pairs indicated by these two curves are the dominant contributors to the stable electromagnetic torques produced in these FSPM machines. The products of the magnitudes of the field harmonic pairs are plotted in the blue curve. With no doubt, this curve can reflect the magnetic coupling of the field harmonic pairs. Apparently, the blue curve has similar pattern to those curves illustrated in Fig. 29. When the ratio of N_s and N_r is near to 1, the magnetic coupling of the field harmonic pair is much stronger than those in the other cases. That is the reason why the number of stator poles should be close to the number of rotor poles when designing FSPM machines.

V. Experimental Verification

As shown in Fig. 31, two sample machines, viz., 12/13 FSPM and 12/26 FSPM machines, are prototyped for experimental verification. Both machines are with exactly the same specifications as listed in Table II, and the numbers of turns per coil are both equal to 100. The differences of these two machines lie

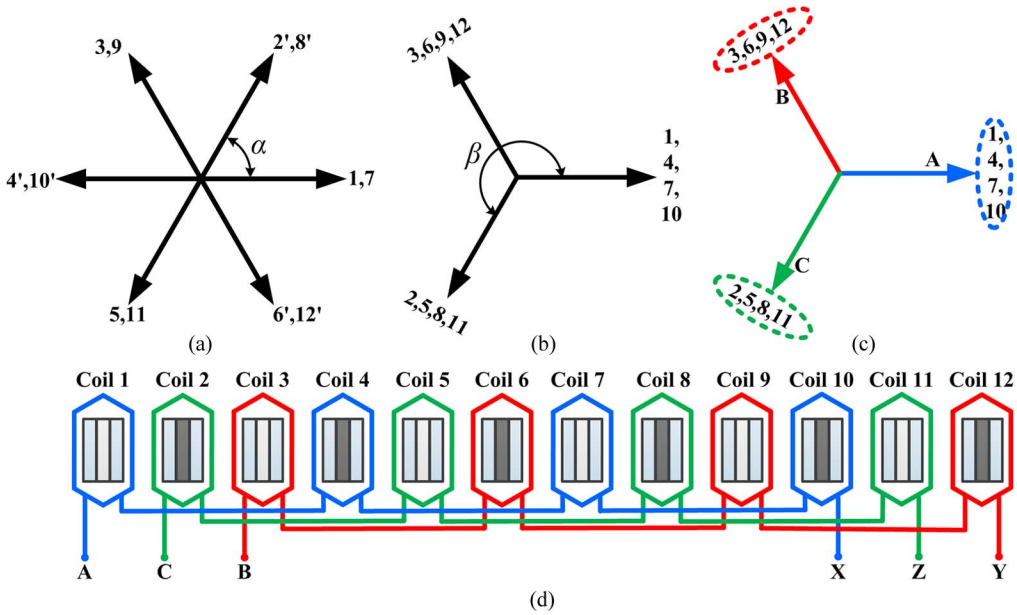

Fig. 26. Winding connection approach (12/26 FSPM machine). (a) Coil-EMF vectors from the generator-oriented perspective. (b) Coil-EMF vectors from the motor-oriented perspective. (c) Three phase coil vectors. (d) Three phase winding connection.

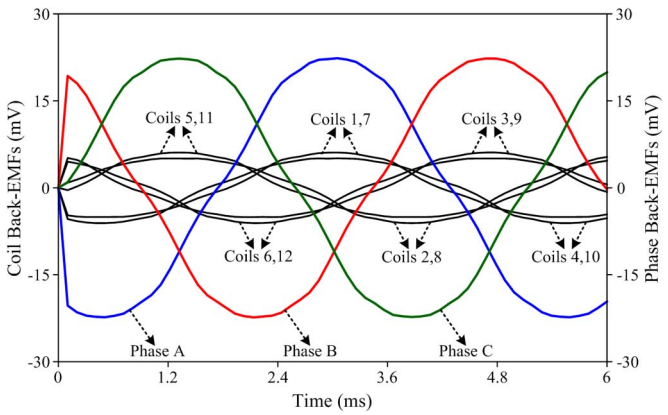

Fig. 27. Back-EMF waveforms of coils and phases (12/26 FSPM machine).

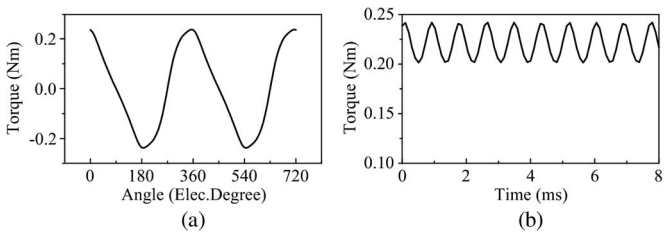

Fig. 28. Performance of electromagnetic torque (12/26 FSPM machine). (a) Torque–angle curve when rotor is kept at standstill. (b) Maximum torque–time waveform with rotor rotating at synchronous speed.

TABLE III
FSPM MACHINES WITH DIFFERENT COMBINATIONS OF N_s AND N_r

N_s	N_r	$P_s = N_s/2$	$P_w = N_r - P_s$	β=360° (P_w / N_s)	Y/N
12	1	6	-5	—	N
12	2	6	-4	—	N
12	3	6	-3	—	N
12	4	6	-2	—	N
12	5	6	-1	—	N
12	6	6	0	—	N
12	7	6	1	30°	Y
12	8	6	2	60°	Y
12	9	6	3	90°	N
12	10	6	4	120°	Y
12	11	6	5	150°	Y
12	12	6	6	180°	N
12	13	6	7	210°	Y
12	14	6	8	240°	Y
12	15	6	9	270°	N
12	16	6	10	300°	Y
12	17	6	11	330°	Y
12	18	6	12	0°	N
12	19	6	13	30°	Y
12	20	6	14	60°	Y
12	21	6	15	90°	N
12	22	6	16	120°	Y
12	23	6	17	150°	Y
12	24	6	18	180°	N
12	25	6	19	210°	Y
12	26	6	20	240°	Y

in the number of rotor poles and the connections of coils, which are illustrated in Figs. 18 and 26, respectively.

Fig. 32 shows the measured phase back EMF waveforms when the rotors rotate at 450 r/min. The magnitudes of back EMF generated by the 12/13 FSPM machine is 28.54 V, while that generated by the 12/26 FSPM machine is 1.95 V. The results calculated by using the FEM are also depicted for comparison, and the corresponding magnitudes are 32.62 and 2.25 V, respectively. The simulation results match very well

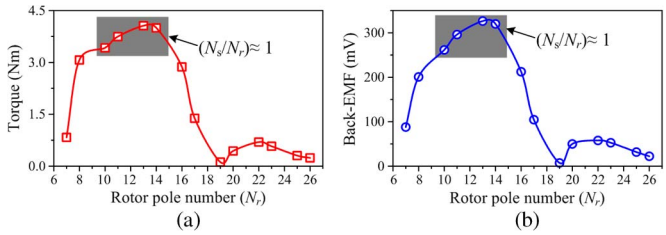

Fig. 29. Comparison of performances. (a) Peak values of stable electromagnetic torques. (b) Magnitudes of phase back EMFs.

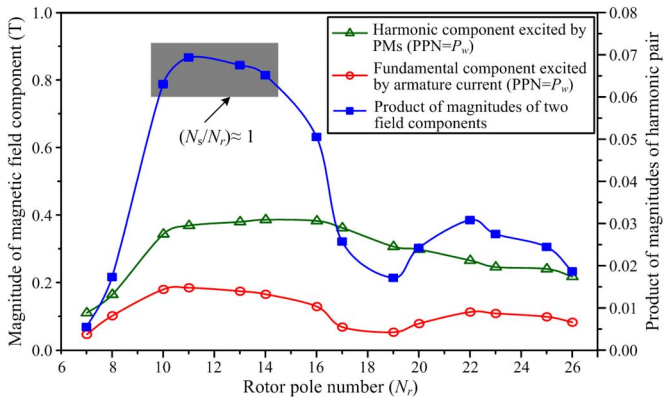

Fig. 30. Comparison of magnitudes of key field components.

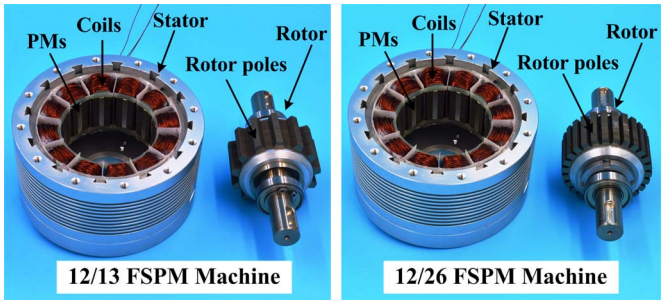

Fig. 31. Two prototype machines: (Left) 12/13 FSPM machine and (right) 12/26 FSPM machine.

with the measured results. Fig. 33 shows the measured peak values of electromagnetic torques with different armature currents. The calculated results are also presented for comparison. When the magnitude of phase current is equal to 3 A, the maximum electromagnetic torques offered by the 12/13 FSPM machine is 3.76 Nm, while that offered by the 12/26 FSPM machine is 0.21 Nm. It can be observed that the simulation results also match very well with the measured results.

The measured results shown in Figs. 32 and 33 demonstrate that, when the number of rotor poles is close to the number of stator poles, the FSPM machine can offer prominent electromagnetic performance.

VI. Conclusion

In this paper, the operating principle of FSPM machines with all poles wound has been elaborated comprehensively from the proposed motor-oriented perspective. Due to the salient

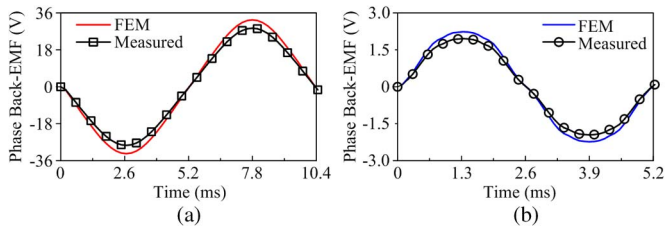

Fig. 32. Results of phase back EMFs. (a) 12/13 FSPM machine. (b) 12/26 FSPM machine.

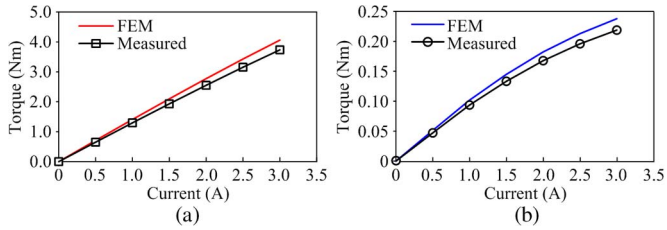

Fig. 33. Results of peak value of electromagnetic torques. (a) 12/13 FSPM machine. (b) 12/26 FSPM machine.

pole structure, magnetic fields excited by PMs and armature currents are modulated based on magnetic gearing effect. In essence, the FSPM machine can be considered as a unique type of flux-modulated machine. The analysis shows that, in the FSPM machine, there are many effective harmonic pairs in the air gap, which can interact with each other so as to generate stable electromagnetic torques. In addition, several key concepts concerning FSPM machines, such as the PPN of PMs, the PPN of armature windings, and the synchronous speed of the armature field, are defined. Based on that, a new approach for determining the connection of coils is built up for the sake of developing stable output torque. This new approach is more consistent with the classical theory of electric machines since there is no need to take into account the polarity of the coils. Case studies based on the FEM simulation and experimental verification demonstrate the validity of the proposed analysis approach. Comparison among sample machines with different combinations of stator pole and rotor pole shows that, when the ratio of N_s and N_r is close to 1, the resulted FSPM machine can offer prominent electromagnetic performance.

References

[1] M. Cheng, W. Hua, J. Zhang, and W. Zhao, "Overview of stator-permanent magnet brushless machines," *IEEE Trans. Ind. Electron.*, vol. 58, no. 11, pp. 5087–5101, Nov. 2011.

[2] R. Antonello, M. Carraro, and M. Zigliotto, "Maximum-torque-per-ampere operation of anisotropic synchronous permanent-magnet motors based on extremum seeking control," *IEEE Trans. Ind. Electron.*, vol. 61, no. 9, pp. 5086–5093, Sep. 2014.

[3] S. E. Rauch and L. J. Johnsom, "Design principles of flux-switching alternators," *AIEEE Trans.*, vol. 74, no. 3, pp. 1261–1268, 1955.

[4] Y. Liao, F. Liang, and T. A. Lipo, "A novel permanent magnet machine with doubly salient structure," *IEEE Trans. Ind. Appl.*, vol. 31, no. 5, pp. 1069–1078, Sep./Oct. 1995.

[5] Z. Zhang, L. Yu, L. Sun, L. Qian, and X. Huang, "Iron loss analysis of doubly salient brushless dc generators," *IEEE Trans. Ind. Electron.*, vol. 62, no. 4, pp. 2156–2163, Apr. 2015.

[6] D. More and B. Fernandes, "Analysis of flux-reversal machine based on fictitious electrical gear," *IEEE Trans. Energy Convers.*, vol. 25, no. 4, pp. 940–947, Dec. 2010.

[7] T. Raminosoa, C. Gerada, and M. Galea, "Design considerations for a fault-tolerant flux-switching permanent-magnet machine," *IEEE Trans. Ind. Electron.*, vol. 58, no. 7, pp. 2818–2825, Jul. 2011.
[8] W. Hua, G. Zhang, and M. Cheng, "Flux-regulation theories and principles of hybrid-excited flux-switching machines," *IEEE Trans. Ind. Electron.*, vol. 62, no. 9, pp. 5359–5369, Sep. 2015.
[9] R. L. Owen, Z. Q. Zhu, and G. W. Jewell, "Hybrid-excited flux-switching permanent-magnet machines with iron flux bridges," *IEEE Trans. Magn.*, vol. 46, no. 6, pp. 1726–1729, Jun. 2010.
[10] Z. Q. Zhu *et al.*, "Analysis of electromagnetic performance of flux-switching PM machines by nonlinear adaptive lumped parameter magnetic circuit model," *IEEE Trans. Magn.*, vol. 41, no. 11, pp. 4277–4287, Nov. 2005.
[11] W. Hua, M. Cheng, Z. Q. Zhu, and D. Howe, "Analysis and optimization of back EMF waveform of a flux-switching permanent magnet motor," *IEEE Trans. Energy Convers.*, vol. 23, no. 3, pp. 727–733, Sep. 2008.
[12] J. T. Chen and Z. Q. Zhu, "Winding configurations and optimal stator and rotor pole combination of flux-switching PM brushless ac machines," *IEEE Trans. Energy Convers.*, vol. 25, no. 2, pp. 293–302, Jun. 2010.
[13] K. Atallah, S. D. Calverley, and D. Howe, "Design, analysis and realisation of a high-performance magnetic gear," *Proc. Inst. Elect. Eng.—Elect. Power Appl.*, vol. 151, no. 2, pp. 135–143, Mar. 2004.
[14] L. Jian and K. T. Chau, "A coaxial magnetic gear with Halbach permanent-magnet arrays," *IEEE Trans. Energy Convers.*, vol. 25, no. 2, pp. 319–328, Jun. 2010.
[15] L. Jian, Y. Shi, J. Wei, and Y. Zheng, "Design and analysis of a direct-drive wind power generator with ultra-high torque density," *J. Appl. Phys.*, vol. 117, 2015, Art. ID. 17A713.
[16] L. Jian, G. Xu, C. Mi, K. T. Chau, and C. C. Chan, "Analytical method for magnetic field calculation in a low-speed permanent-magnet harmonic machine," *IEEE Trans. Energy Convers.*, vol. 26, no. 3, pp. 862–870, Sep. 2011.
[17] L. Jian *et al.*, "A novel dual-permanent-magnet-excited machine for low-speed large-torque applications," *IEEE Trans. Magn.*, vol. 49, no. 5, pp. 2381–2384, May 2013.
[18] B. Bai, P. Zheng, C. Tong, Z. Song, and Q. Zhao, "Characteristic analysis and verification of the magnetic-field-modulated brushless double-rotor machine," *IEEE Trans. Ind. Electron.*, vol. 62, no. 7, pp. 4023–4033, Jul. 2015.
[19] R. Cao, M. Cheng, C. Mi, and W. Hua, "Influence of leading design parameters on the force performance of a complementary and modular linear flux-switching permanent-magnet motor," *IEEE Trans. Ind. Electron.*, vol. 61, no. 5, pp. 2165–2175, May 2014.

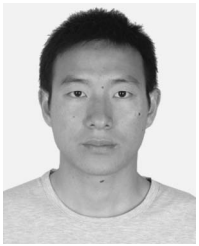

Yujun Shi (M'15) received the B.Sc. degree from Hubei Polytechnic University, Huangshi, China, in 2010 and the M.Sc. degree from Jiangsu University, Zhenjiang, China, in 2013.

From 2013 to 2014, he was a Research Assistant in the Shenzhen Institutes of Advanced Technology, Chinese Academy of Sciences, Shenzhen, China. He is currently a Research Assistant with the Department of Electrical and Electronic Engineering, South University of Science and Technology of China, Shenzhen, China. His research interests include the design, analysis, and optimization of permanent-magnet electric machines.

Linni Jian (SM'14) received the B.Eng. degree from Huazhong University of Science and Technology, Wuhan, China, in 2003, the M.Eng. degree from the Institute of Electrical Engineering, Chinese Academy of Sciences, Beijing, China, in 2006, and the Ph.D. degree from The University of Hong Kong, Pokfulam, Hong Kong, in 2010.

He is currently an Assistant Professor in the Department of Electrical and Electronic Engineering, South University of Science and Technology, Shenzhen, China. His research interests include the areas of electric drives, power electronics, and smart grids. In these areas, he has published more than 60 refereed technical papers, one monograph, and several book chapters. He is also the holder of more than 20 patents.

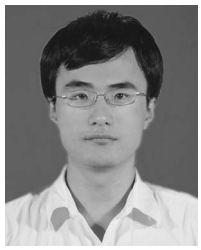

Jin Wei received the B.Sc. and M.Sc. degrees from Hefei University of Technology, Hefei, China, in 2009 and 2012, respectively.

From 2012 to 2014, he was a Research Assistant in the Shenzhen Institutes of Advanced Technology, Chinese Academy of Sciences, Shenzhen, China. He is currently a Research Assistant with the Department of Electrical and Electronic Engineering, South University of Science and Technology of China, Shenzhen, China. His research interests mainly include mechanical design and manufacturing of permanent-magnet electric machines.

Ziyun Shao (M'12) received the B.Eng. degree from Shandong University, Jinan, China, in 2005, the M.Sc. degree from the Hong Kong University of Science and Technology, Hong Kong, in 2007, and the Ph.D. degree from The University of Hong Kong, Pokfulam, Hong Kong, in 2011.

She is currently a Lecturer in the School of Mechanical and Electrical Engineering, Guangzhou University, Guangzhou, China. Her research interests are in the areas of mathematical modeling and optimization and their applications in engineering problems. In these areas, she has published several technical papers and one book chapter.

Wenlong Li received the B.Eng. degree from Sichuan University, Chengdu, China, in 2005, the M.Eng. degree from the University of Science and Technology of China, Hefei, China, in 2008, and the Ph.D. degree from The University of Hong Kong, Pokfulam, Hong Kong, in 2012, respectively.

He is currently a Postdoctoral Researcher with the Department of Electrical and Electronic Engineering, The University of Hong Kong. His research interests are in the areas of electric drives, electric vehicles, and renewable energy harvesting. In these areas, he has published more than 20 refereed technical papers.

C. C. Chan (F'92) received the B.Sc., M.Sc., and Ph.D. degrees in electrical engineering, respectively, from the China University of Mining and Technology, Beijing, China, Tsinghua University, Beijing, China, and The University of Hong Kong, Pokfulam, Hong Kong, in 1957, 1959, and 1982, respectively.

He is currently an Honorary Professor and the former Head of the Department of Electrical and Electronic Engineering, The University of Hong Kong. He has had more than ten years of industrial experience and more than 35 years of academic experience. He is the Founding President of the International Academy for Advanced Study, China, the Cofounder and Rotating President of the World Electric Vehicle Association, and the President of the Electric Vehicles Association of Asia Pacific.

Prof. Chan is a Fellow of the Royal Academy of Engineering, U.K., the Chinese Academy of Engineering, the Ukraine Academy of Engineering Sciences, the Institution of Engineering and Technology, U.K., and the Hong Kong Institution of Engineers.